

Fluorescence Lifetime Enhancement of Organic Chromophores Attached to Gold Nanoparticles

Florencio E. Hernández,^{*,†} Shenjiang Yu, Marisol García, and Andrés D. Campiglia

Department of Chemistry, University of Central Florida, P.O. Box 162366, Orlando, Florida 32816-2366

Received: February 15, 2005; In Final Form: March 22, 2005

We present for the first time experimental evidence of fluorescence lifetime enhancement of organic chromophores attached to metal nanospheres via radiative decay engineering. The hybrid system (HS) was a modified “diconjugated” molecular probe, 4-acetamido-4'-maleimidylstilbene-2,2'-dithiol (AMDT), covalently bound to the surface of 5-nm-diameter Au nanospheres by its two sulfur atoms, at a distance $d < 1$ nm and with its molecular axis parallel to the surface of the nanoparticle surface. We measured a fluorescence lifetime increase of a factor of 2 at room temperature ($\tau_{\text{AMDT}} = (4.32 \pm 0.10)$ ns and $\tau_{\text{HS}} = (8.73 \pm 0.23)$ ns) and a factor of 3.4 at 4.2 K ($\tau_{\text{AMDT}} = (2.64 \pm 0.07)$ ns and $\tau_{\text{HS}} = (7.96 \pm 0.14)$ ns). We also found that the fluorescence quantum yield of this hybrid system is not reduced, proof of a weak energy transfer between the molecular probe and the nanoparticle. These results demonstrate that a molecular dipole oriented parallel to the metal surface tends to be reduced by the coupling with its image.

1. Introduction

The extraordinary physical-chemical properties of metal particles as they approach the nanometer scale have increased the interest of physicists and chemists in nanoscience.¹ Nanoparticles have found many applications in catalysis,² environmental³ and biological labeling and sensing,^{4–7} surface Raman scattering,⁸ nonlinear absorption processes,⁹ photonics,¹⁰ and optoelectronics.¹¹ Nanoscience is also having an impact in biophotonics through radiative decay engineering (RDE) of organic dye molecules in the close vicinity of conducting metal surfaces or covalently attached to them.^{12–14}

It has been demonstrated that fluorescence intensity can be enhanced orders of magnitude when organic dyes are near metal thin films and nanoparticles.^{15,16} This is the outcome of the intensification of the incoming electric field at the surface plasmon resonance (SPR) and the increase of the radiative decay rate of the fluorophore due to the presence of the metal surface.¹⁶ Reports have also shown that fluorescence can be quenched if the fluorophores are within the Forster radius with respect to the metal surface, where energy transfer becomes very important.^{17,18} These effects are a consequence of the dipole–dipole interaction between the dye molecules and the metal surface. The main critical parameters that modify the spontaneous rate of emission of organic dyes near metal nanoparticles are the location of the dye around the particle, its separation from the metal surface, and the molecular dipole orientation with respect to the particle surface.¹⁹

Barnes has described the modification of spontaneous emission produced by a planar metal surface using photonic mode density as decay routes.¹⁹ He showed that in the small separation regime, i.e., less than 100 nm from a planar metal surface, perpendicular orientation of the molecular dipole of emitters (considered as a forced damped dipole oscillator) with respect to the surface tends to be enhanced by its image dipole reflected

from the metal surface, while the parallel one is canceled out. Therefore, the emission rate can be either increased or decreased for a perpendicular or parallel molecular dipole orientation, respectively. Chew calculated the transition rate for the two polarizations of an oscillator atom outside a perfectly conducting sphere of radius r placed at a distance d_r from the center of the sphere.²⁰ Similar results to those observed with the planar metal surface¹⁹ were obtained. As d_r approaches r , the emission rate increases for perpendicular polarization and decreases for parallel polarization. Experiments showing a decrease of fluorescence lifetimes of dye molecules in the immediate vicinity of metal surfaces have been extensively reported,^{15,16,18} but there is no experimental evidence of fluorescence lifetime enhancement of organic dyes close to metal surfaces.

In this article, we report the first experimental evidence showing a fluorescence lifetime enhancement of an organic dye chemically attached to the surface of spherical nanoparticles. The chromophore consists of a hybrid system (HS) containing a modified dithiol molecular probe attached to the surface of 5-nm-average-diameter gold nanospheres (Au-Np). The schematic diagram shown in Figure 1 depicts the molecular structure of the fluorescent probe (4-acetamido-4'-maleimidylstilbene-2,2'-dithiol (AMDT)) and the resulting HS. The molecular axis of the probe is parallel to the surface of the spherical nanoparticle, and the distance between them is shorter than 1 nm. We also show that the fluorescence quantum yield of the probe remains constant upon attachment to the surface of the nanoparticle as a result of weak energy transfer between them. Our results demonstrate that a molecular dipole oriented parallel to the metal surface tends to be reduced by its dipole image on the reflecting surface, far from the SPR.

2. Experimental Section

Gold Nanoparticles. Gold nanospheres were synthesized with a 5-nm average diameter (<10% size distribution) following the wet chemical method of Turkevich et al.^{21,22} The nanoparticle size and distribution were determined by transmission electron microscopy using an FEI Tecnai F30 TEM. The

* Author to whom correspondence should be addressed. Phone: (407) 823-0843. Fax: (407) 823-2252. E-mail: florenzi@mail.ucf.edu.

† Also with the College of Optics and Photonics/CREOL/FPCE.

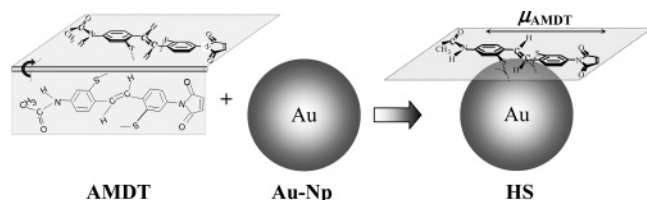


Figure 1. Structure of the 4-acetamido-4'-maleimidylstilbene-2,2'-dithiol (AMDT), schematic representation of the 3.5-nm-diameter gold spherical nanoparticles (Au-Np), and biattached AMDT onto a gold nanoparticle hybrid system (HS). The red double side arrow represents the plane of the molecular dipole moment μ_{AMDT} .

gold nanospheres average diameter met the theoretical model of Dulkeith et al.,²³ which predicts minimum radiative decay rate values (or maximum fluorescence lifetime enhancements) for organic dyes attached to 3–5-nm-diameter Au-Np.

Fluorescence Probe. AMDT was prepared from a commercially available source (4-acetamido-4'-maleimidylstilbene-2,2'-disulfonic acid, disodium salt) from Molecular probes IDT, following a previously reported procedure using phosphorus pentasulfide and LiAlH_4 .²⁴ The characterization of the new product was done by NMR with a Varian 500 MHz Unity NMR Spectrometer. The doublet at 3.85 ppm confirmed the reduction of the disulfonic acid and the formation of the dithiol homologues. The probe was chosen on the assumption that the two thiol groups would force, through chemical bonding, a parallel orientation of the molecular moiety with respect to the surface of the particle. Because the other possibility, i.e., monoattachment of AMDT molecules via one thiol group, would only occur at a later stage of the functionalization process, the resulting HS should consist of a predominant population of biattached AMDT molecules on the surface of the particles. It is important to note that the fraction of monoattached molecules should not have a noticeable effect on the overall orientation dipole moment of AMDT molecules because their proximity to the surface of the metal should restrict their orientation and their dipole moment to a parallel position with respect to the metal surface.

Hybrid System. AMDT molecules were incorporated onto Au-Np following the thiolate chemistry cape method developed by Brust.²⁵ We mixed 5 mL of the Au-Np suspension with 0.6 mL of a 5.04×10^{-4} M solution of AMDT in octane for 90 min. Then, we added 0.6 mL of octane and 16 mg of KI to the aqueous phase to “salt out” the hybrid system AMDT–Au-Np. An identical solution of AMDT with no Au-Np was prepared for comparison under identical experimental conditions. Nanoparticle functionalization was confirmed by the presence of the surface plasmon resonance band ($\lambda_{\text{SPR}} = 526$ nm) in the layer of organic solvent (octane) used to extract the HS from the original aqueous solution. The absence of the SPR band in the organic layer, after an attempt to extract Au-Np from the aqueous phase using pure octane, demonstrated that in the absence of AMDT gold nanoparticles were not transferred to the organic phase. Absorbance measurements were carried out with a single-beam spectrophotometer (model Cary 50, Varian) equipped with a 75-W pulsed xenon lamp, 2-nm fixed band pass, and 24 000 nm min^{-1} maximum scan rate.

Initial Survey of Spectral Characteristics at Room Temperature. Steady-state excitation and fluorescence spectra were recorded from undegassed solutions with standard quartz cuvettes (1 cm \times 1 cm) using a commercial spectrofluorimeter (Photon Technology International). The excitation source was a continuous-wave 75-W xenon lamp with broadband illumination from 200 to 2000 nm. The excitation and the emission monochromator had the same reciprocal linear dispersion (4 nm

mm^{-1}) and accuracy (± 1 nm with 0.25 nm resolution). The gratings (1200 grooves mm^{-1}) were blazed at 300 and 400 nm, respectively. Detection was made with a photomultiplier tube (PMT, model 1527) with wavelength range from 185 to 650 nm. In the photon counting mode, the maximum count rate was 4 MHz, rise time 20 ns, and fall time 100 ns with a 220 ns pulse width. The instrument was computer-controlled using commercial software (Felix32) specifically designed for the system.

Time-Resolved Fluorescence Measurements at Room and Low Temperatures. The instrumentation for time-resolved fluorescence measurements was developed in house by Campiglia and co-workers. Its performance with respect to accuracy and precision has been previously compared to conventional approaches.^{26,27} Sample excitation was carried out by directing the output of a Northern Lights tunable dye laser (Dakota Technologies, Inc.) through a KDP frequency-doubling crystal. The dye laser was operated on LDS 698 (Exiton), and it was pumped with the second harmonic of a 10 Hz Nd:YAG Q-switched solid-state laser (Big Sky Laser Technologies). Time-resolved fluorescence detection was performed with a multichannel detector consisting of a front-illuminated intensified charge fiber-coupled device (ICCD, ANDOR Technology). The minimum gate time full width at half-maximum (fwhm) of the intensifier was 2 ns, and the CCD active area was 690 pixels \times 256 pixels (26 mm^2 pixel size photocathode). The ICCD was mounted at the exit focal plane of a spectrograph (SPEX 270M) equipped with a grating (1200 grooves mm^{-1}) blazed at 500 nm. The system was used in the external trigger mode. The gate delay, width, and step were controlled with a digital delay generator (DG535, Stanford Research System, Inc.) via a GPIB interface. Custom Labview software (National Instruments) was developed in house for complete instrumental control and data collection.²⁷

Sample measurements were made with the aid of a fiber optic probe. The probe consisted of an assembly with one excitation and six collection fibers fed into a 1.25-m-long section of copper tubing. All of the fibers were 3-m-long and 500- μm core-diameter silica-clad silica with polyimide buffer coating (Polymicro Technologies, Inc.). At the analysis end, the excitation and emission fibers were arranged in a conventional six-around-one configuration, bundled with vacuum epoxy (Torr-Seal, Varian), and fed into a metal sleeve for mechanical support. The copper tubing was flared, stopping a swage nut tapped to allow for the threading of a 0.75-mL polypropylene sample vial. At the instrument end, the excitation fiber was positioned in an ST connection and aligned with the beam of the tunable dye laser while the emission fibers were bundled with vacuum epoxy in a slit configuration, fed into a metal sleeve, and aligned with the entrance slit of the spectrometer. Unless otherwise noted, measurements were made using 250 μL of undegassed sample. Freezing to 77 and 4.2 K was accomplished by lowering the fiber optic probe into liquid nitrogen and liquid helium, respectively. The liquid helium was contained in a 60-L Dewar. Complete sample freezing took less than 90 s.

Fluorescence lifetimes were determined via a three-step procedure: (1) collection of full sample and background wavelength–time matrix (WTM); (2) subtraction of the background decay curve from the fluorescence decay curve at the wavelength of maximum fluorescence for each analyte; (3) fitting of the background corrected data to single exponentials. Origin software (version 5, Microcal Software, Inc.) was used for curve fitting of fluorescence lifetimes. Fitted decay curves ($y = y_0 + A_1 \exp^{-(x-x_0)/\tau_1}$) were obtained by fixing y_0 and x_0 at

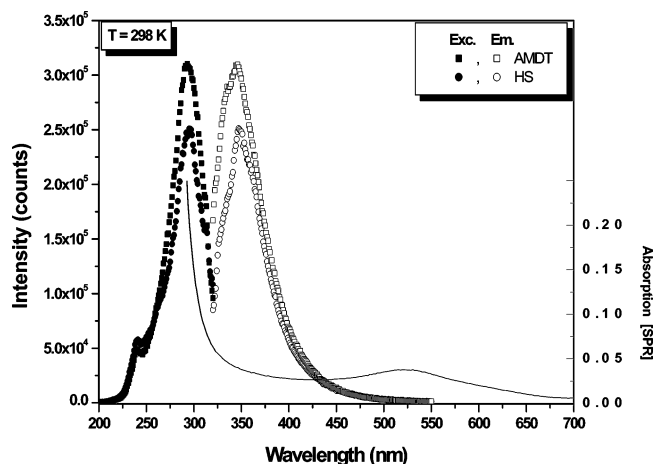


Figure 2. Excitation and emission spectra of AMDT and HS at 298 K. Absorption spectrum of Au-Np (surface plasmon resonance band with $\lambda_{\text{max}} = 526$ nm) (right-side axis).

a value of zero. It is important to note that the accuracy of this procedure has been previously confirmed.^{26,27}

3. Results and Discussions

Figure 2 shows the excitation and emission spectra of AMDT and HS at room temperature (RT) as well as the typical surface plasmon resonance band of Au-Np present in the HS. The excitation and emission spectra of free AMDT and attached AMDT have the same profile. This is a strong indication that the functionalization and attachment of AMDT to the Au-Np nanoparticles did not modify the molecular structure of the fluorophore. The fluorescence intensity of free AMDT is approximately 24% higher than the fluorescence intensity of HS. The higher intensity is mainly attributed to the higher concentration of free AMDT in the octane solution. Although the original AMDT concentration for the synthesis of HS was adjusted to provide a final concentration of attached AMDT equal to the concentration of free AMDT in octane (2.5×10^{-4} M), the reaction does not provide a 100% yield, and some AMDT is certainly lost in the synthesis by the HS. Another contributing factor for the lower fluorescence intensity of AMDT in the HS is the absorption of gold within the emission range of the fluorophore. The presence of gold nanoparticles in solution might account for the absorption of a fraction of fluorescence photons. Quantum yield and lifetime measurements presented here will show that no significant quenching occurs due to energy transfer from AMDT to the metal surface.

Comparison of spectra in Figure 2 also shows that sample excitation at 296.7 nm, the maximum excitation wavelength of AMDT and HS, promotes negligible enhanced absorption via SPR from Au-Np. This excitation wavelength does not overlap with the SPR absorption band at $\lambda_{\text{max}} = 526$ nm. It is also important to note that, under steady-state measurement conditions, weak fluorescence emission was observed from an Au-Np suspension. This emission, which spectrally overlapped with AMDT fluorescence, results from the excitation of electron-hole pairs in gold particles.²³ Because its decay is relatively fast (picosecond time regime) in comparison to the fluorescence lifetime of AMDT (nanosecond time domain), its potential interference was time-discriminated with the laser system.

Figure 3 displays the fluorescence wavelength-time matrix (WTM) of AMDT and HS collected with the laser system and the fiber optic probe.²⁷ Each spectrum in the WTM resulted from the accumulation of 100 laser pulses collected at different

delays from the excitation pulse. The inset in Figure 3 shows the normalized decay curves obtained for free AMDT and the probe in the HS. Both WTMs were recorded from octane solutions at room temperature (298 K). The lifetime values (τ_i) stripped from the WTMs are presented in Table 1. The fluorescence lifetime of AMDT in the HS ($\tau_{\text{HS}} = 8.73 \pm 0.23$ ns) is considerably longer ($\sim 2\times$) than the lifetime of the free probe ($\tau_{\text{AMDT}} = 4.32 \pm 0.10$ ns). On the basis of this behavior, one would predict a quenching effect on the fluorescence of the probe in the HS. However, the quenching was not observed. Table 2 reports the fluorescence quantum yields of AMDT and HS in octane at 298 K. Their values were calculated by the standard method using phenanthrene in octane as the reference standard (quantum yield $Q_{\text{st}} = 0.125 \pm 0.005$).²⁸ Within 95% of probability ($\alpha = 0.05$), their average quantum yields based on three experimental values ($N = 3$) were statistically equivalent.²⁹

The lack of fluorescence quenching associated to the significant change in fluorescence lifetimes leads us to postulate a parallel orientation of the dipole moment of AMDT with respect to the metal surface, a situation where the dipole moment of the probe is reduced by its dipole image. This observation agrees with a previous report on the theoretical aspects of fluorescence deactivation mechanisms of organic dyes covalently attached to planar and spherical surfaces. According to Barnes and Chew,^{19,20} molecular dipoles that align parallel to a reflecting metal surface tend to cancel out with their reflected dipole images. The reduction of the dipole strength leads to longer fluorescence lifetimes and shorter radiative decay rates. If the probe molecules were oriented with their dipole moments perpendicular to the metal surface, then we should have observed fluorescence quenching as a result of an enhancement of the resonance dipole-dipole interaction process.^{19,20,30}

In a related article, Dukeith and co-workers²³ reported experimental evidence on the decrease of the radiative decay rate of dye molecules chemically monoattached to a metal surface at expenses of their nonradiative decay rate. The combination of these two effects led to fluorescence quenching due to energy transfer from the dye to the metal.²³ The results presented in Table 2 predict a different scenario for dye molecules chemically biattached to a metal surface. The statistical comparison ($\alpha = 0.05$; $N = 3$)²⁹ of the radiative (Γ_i) and nonradiative ($k_{\text{nr}(i)}$) decays of AMDT and HS shows a decrease of both decay rates. We attribute this behavior to the reduced number of degrees of freedom resulting from the biochemical attachment of AMDT to Au-Np.

Another possible explanation for the fluorescence lifetime enhancement could be attributed to the blocking of the internal conversion pathway accompanied by a photoinduced trans \rightarrow cis isomerization on AMDT attached to Au-Np. To discard any misinterpretation of our results, the fluorescence lifetimes of AMDT and HS were also measured at low temperature. Figure 4 shows the normalized fluorescence intensity versus time of frozen AMDT and HS at liquid nitrogen (top panel) and liquid helium (bottom panel) temperatures. The 77 and 4.2 K fluorescence lifetime values are shown in Table 2. The 77 K quantum yields of AMDT and HS and their respective radiative and nonradiative decay rates are shown in Table 2. Similar to room-temperature measurements, the 77 K quantum yields of AMDT and HS were calculated by the standard method,²⁸ using an octane solution of anthracene ($Q = 0.206 \pm 0.019$; $N = 3$) as the reference standard. The 4.2 K fluorescence quantum yields were not measured because of the lack of appropriate reference standards.

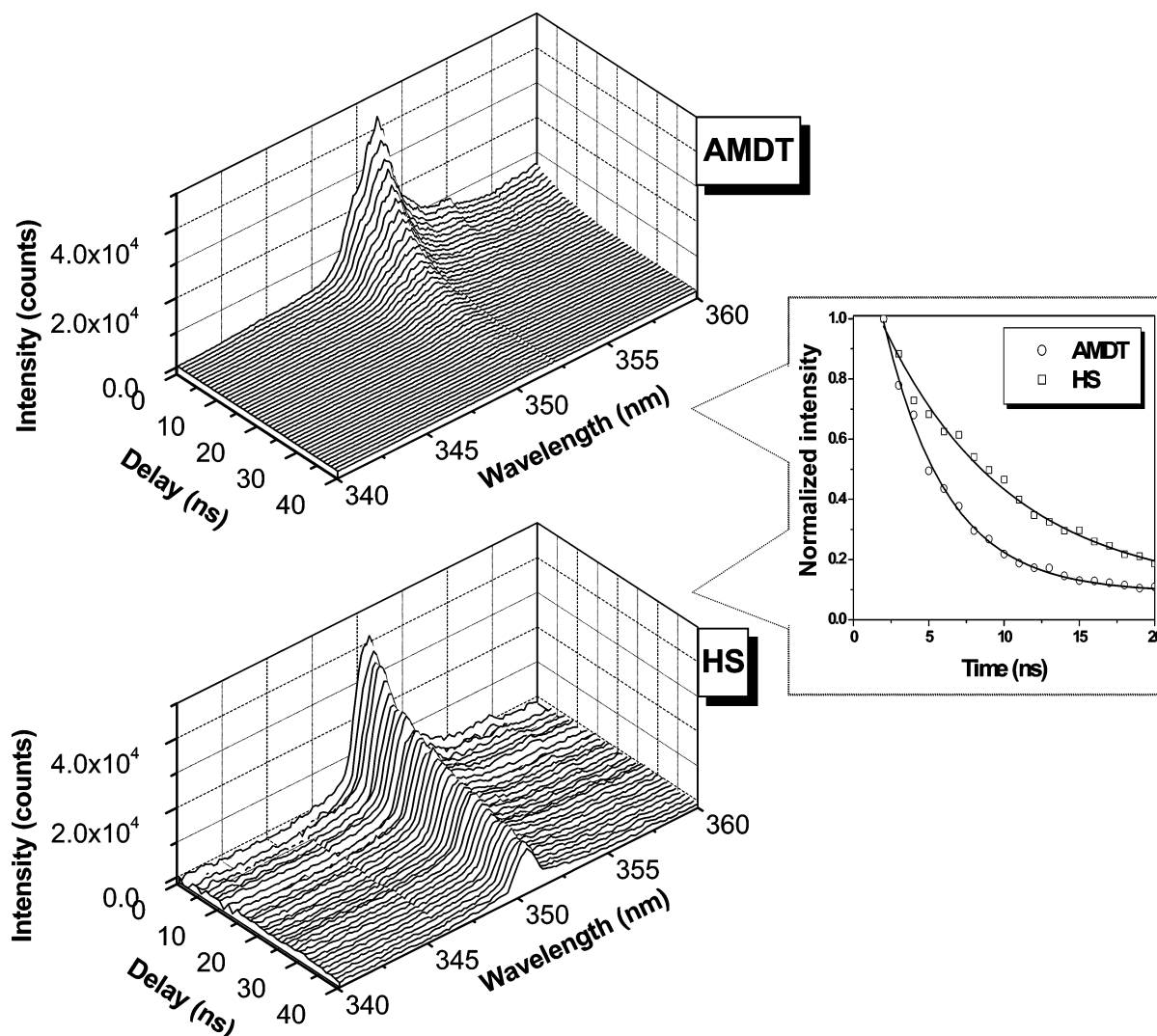


Figure 3. Wavelength–time matrix of AMDT (top panel) and HS (bottom panel) in octane solutions at 298 K. Initial delay time was 2 ns, gate width 200 ns, and delay step 2 ns. Inset: Normalized intensity vs delay time (ns) of AMDT (○) and HS (□). Solid lines are the monoexponential fittings of the experimental data yielding $\tau_{\text{AMDT}} = 4.32 \pm 0.10$ ns and $\tau_{\text{HS}} = 8.73 \pm 0.23$ ns.

TABLE 1: Measured Fluorescence Lifetime of AMDT and HS at 298, 77, and 4.2 K

	τ^a (ns)		
	298 K	77 K	4.2 K
AMDT	4.32 ± 0.10	3.61 ± 0.05	2.34 ± 0.07
HS	8.73 ± 0.23	8.22 ± 0.19	7.96 ± 0.14

^a Lifetime values and standard deviations correspond to the averages of three single measurements taken from three aliquots of the same sample.

Schulte-Frohlinde et al. studied the *trans* \rightarrow *cis* isomerization quantum yield ($Q_{\text{T} \rightarrow \text{C}}$) temperature dependence of stilbene derivatives.³¹ It was demonstrated that $Q_{\text{T} \rightarrow \text{C}}$ can be as low as 0.006 at 93 K. The authors³¹ concluded that frozen stilbene molecules do not experience significant photoisomerization at low temperatures. The main species in frozen solutions is the *trans* isomer. Since AMDT also belongs to the stilbene family, we can postulate that the main isomer present in the frozen solutions of the free probe is *trans*-AMDT. Comparison of the fluorescence lifetimes of AMDT in Table 1 shows a significant decrease when lowering the temperature from 298 to 77 K (in ca. 17%) and from 298 to 4.2 K (in ca. 46%). This is attributed to the restriction of the molecular degrees of freedom when *trans*-AMDT is frozen. A similar argument can be done for

HS. In this case, however, the fluorescence lifetime decreases only 9%. This is in agreement with the higher restriction of the molecular degrees of freedom experienced by AMDT molecules when attached to Au–Np.

The quantum yields at room temperature and at 77 K are statistically different ($\alpha = 0.05$; $N = 3$).²⁹ As expected, lowering the temperature enhances the fluorescence emission of both AMDT and HS. Interesting to note is the fact that the difference between the 77 K and the room-temperature quantum yields (0.015) is the same for both species. This result was somehow surprising because a higher reduction of degrees of freedom was expected in the case of the free probe. In light of our results, we attribute the observed phenomenon to the lack of strong rotational motion of free AMDT at room temperature around its central double bond. Schulte-Frohlinde and co-workers demonstrated that in stilbene-based molecules with acceptor group substituents in positions 4 and 4', the predominant isomer in liquid solutions is *trans*.³¹ AMDT belongs to this family of stilbenes with its moderate attractor acetamide and succinidyl ester groups in positions 4 and 4'. As a matter of fact, lowering the temperature to 77 K does not cause a drastic effect in any of the nonradiative constants. Measurements of the quantum yield at 4.2 K were not possible because of the lack of an appropriate standard.

TABLE 2: Measured Quantum Yields (Q_i)^a and Estimated Γ_{0i} ^b and $k_{nr(i)}$ ^c Decay Rates at 298 and 77 K

	298 K			77 K		
	Q_i	$\Gamma_{0i} \times 10^7 (s^{-1})$	$k_{nr(i)} \times 10^7 (s^{-1})$	Q_i	$\Gamma_{0i} \times 10^7 (s^{-1})$	$k_{nr(i)} \times 10^7 (s^{-1})$
AMDT	0.042 ± 0.004	1.00 ± 0.10	22.86 ± 0.57	0.057 ± 0.008	1.60 ± 0.14	26.10 ± 0.41
HS	0.046 ± 0.004	0.55 ± 0.09	11.30 ± 0.31	0.061 ± 0.009	0.74 ± 0.15	11.40 ± 0.31

^a Quantum yields and standard deviations represent the averages of three single measurements taken from three aliquots of the same sample. Calculation of standard deviations includes propagation of errors throughout the entire experimental procedure. ^b Γ_{0i} = radiative decay rate. This rate was calculated substituting the experimental quantum yields (Q_i) and the lifetime values (τ_i) in the following formulas: $\Gamma_{0i} = Q_i \times \tau_{0i}^{-1}$ and $\tau_{0i} = \tau_i / Q_i$. ^c $k_{nr(i)}$ = nonradiative decay rate. This rate was calculated based on the equation $\Gamma_f = \Gamma_{0i} + k_{nr(i)}$, where Γ_f is the fluorescence decay rate calculated as $\Gamma_f = Q_i \times \tau_i^{-1}$. All standard deviations included the propagation of error throughout the entire experimental procedure.

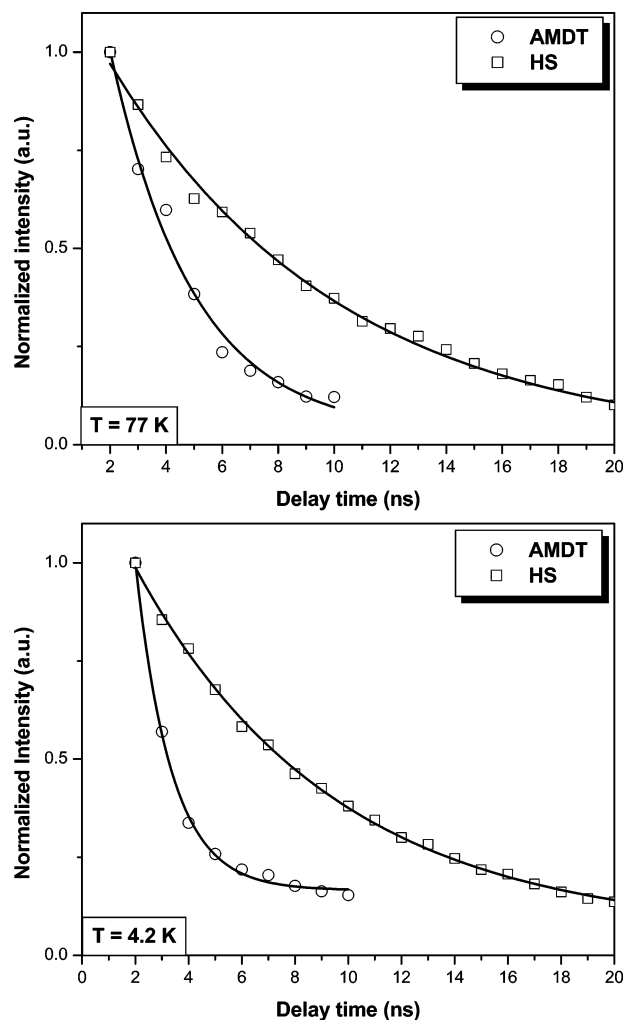


Figure 4. Normalized intensity vs delay time (ns) of AMDT (○) and HS (□). Solid lines are the monoexponential fittings of the experimental data yielding $\tau_{AMDT} = 3.61 \pm 0.05$ ns and $\tau_{HS} = 8.22 \pm 0.19$ ns at 77 K and $\tau_{AMDT} = 2.64 \pm 0.07$ ns and $\tau_{HS} = 7.96 \pm 0.14$ ns at 4.2 K.

Figure 5 shows the two-dimensional fluorescence spectra of AMDT and HS at 77 K. Similar spectral profiles were obtained at room temperature and 4.2 K. Their remarkable similarity at all temperatures is compelling evidence that the chemical bonding of the probe to the metal surface of the particle does not considerably change the molecular moiety of the fluorophore. On the other end, the fluorescence lifetimes of AMDT and HS were different at all temperatures. The difference between fluorescence lifetimes can then be attributed to dipole–dipole interaction between the chromophore dipole moment and its image on the surface of the metal nanoparticle.

It is important to note that there was no evidence of phosphorescence from AMDT and HS. This was somehow expected because the absence of heavy atoms in AMDT reduces the probability of intersystem crossing between S_1 and the triplet

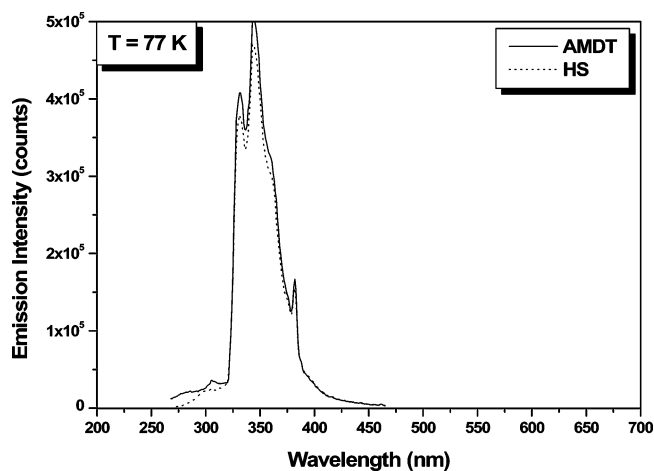


Figure 5. Emission spectra of AMDT (●) and HS (□) at 77 K.

state manifold ($S_1 \rightarrow T_n$). Although the deactivation of S_1 via external conversion might play an important role at room temperature, lowering the temperature to 77 and 4.2 K showed no appearance of phosphorescence. The possibility of oxygen quenching at low temperature was eliminated with several thawing cycles prior to measurements.

4. Conclusion

We have provided the first experimental evidence that a molecular dipole oriented parallel to a noble metal surface tends to be reduced by the coupling with its image. The dipole–dipole coupling enhances the fluorescence lifetime of the organic chromophore in the close vicinity of metal nanoparticles. For AMDT, our experiments showed a lifetime enhancement of $2\times$ at room temperature and $3.4\times$ at liquid helium temperature. A weak energy transfer between the molecular probe and the nanoparticle was corroborated by observing no reduction on the fluorescence quantum yield on the hybrid system. An increase in the quantum yield of AMDT and HS as the temperature was decreased validates the increase of the radiative decay rate in both systems.

Acknowledgment. F.E.H acknowledges the University of Central Florida (In-House Award 11649003) for financial support. A.D.C. acknowledges the National Science Foundation (CHE-0138093) for financial support.

References and Notes

- (1) Kamat, P. V. *J. Phys. Chem. B* **2002**, *106*, 7729.
- (2) Valden, M.; Lai, X.; Goodman, D. W. *Science* **1998**, *281*, 1647.
- (3) Minunni, M.; Mascini, M. *Anal. Lett.* **1993**, *26*, 1441.
- (4) Nicewarner-Peña, S. R.; Freeman, R. G.; Reiss, B. D.; He, L.; Peña, D. J.; Walton, I. D.; Cromer, R.; Keating, C. D.; Natan, M. J. *Science* **2001**, *294*, 137.
- (5) Bruchez, M., Jr.; Moronne, M.; Gin, P.; Weiss, S.; Alivisatos, A. P. *Science* **1998**, *281*, 2013.

- (6) Grate, J. W.; Nelson, D. A.; Skaggs, R.; Synovec R. E.; Gross, G. M. Metal Nanoparticles Protected with Monolayers: Applications for Chemical Vapor Sensing and Gas Chromatography. In *Encyclopedia of NanoScience and Nanotechnology*; Marcel Dekker: New York, 2004.
- (7) Zhang, J.; Malicka, J.; Gryczynski, I.; Lakowicz, J. R. *Anal. Biochem.* **2004**, *330*, 81.
- (8) Nie, S.; Emory, S. R. *Science* **1997**, *275*, 1102.
- (9) Kano, H.; Kawata, S. *Opt. Lett.* **1996**, *21*, 1848.
- (10) Maier, S. A.; Brongersma, M. L.; Kik, P. G.; Meltzer, S.; Requicha, A. A. G.; Atwater, H. A. *Adv. Mater.* **2001**, *13*, 1501.
- (11) Wertheim, G. K.; Diczynski, S. B.; Youngquist, S. E. *Phys. Rev. Lett.* **1983**, *51*, 2310.
- (12) Lakowicz, J. R. *Anal. Biochem.* **2001**, *298*, 1.
- (13) Dubertret, B.; Calame, M.; Libchaber, A. J. *Nat. Biotechnol.* **2001**, *19*, 365.
- (14) Thomas, K. G.; Kamat, P. V. *Acc. Chem. Res.* **2003**, *36*, 888.
- (15) Drexhage, K. H. *Prog. Opt.* **1974**, *12*, 165.
- (16) Lakowicz, J. R.; Shen, Y.; D'auria, S.; Malicka, J.; Fang, J.; Gryczynski, Z.; Gryczynski, I. *Anal. Biochem.* **2002**, *301*, 261.
- (17) Camplon, A.; Gallo, A. R.; Harris, C. B.; Robota, H. J.; Whitemore, P. M. *Chem. Phys. Lett.* **1980**, *73*, 447.
- (18) Chance, R. R.; Prock, A.; Silbey, R. *Adv. Chem. Phys.* **1978**, *37*, 1.
- (19) Barnes, W. L. *J. Mod. Opt.* **1998**, *45*, 661.
- (20) Chew, H. J. *Chem. Phys.* **1987**, *87*, 1355.
- (21) Turkevich, J.; Stevenson, P. C.; Hiller, J. *Discuss. Faraday Soc.* **1951**, *11*, 55.
- (22) Frens, G. *Nature, Phys. Sci.* **1973**, *241*, 20.
- (23) Dulkeith, E.; Morteau, A. C.; Niedereichholz, T.; Klar, T. A.; Feldmann, J.; Levi, S. A.; van Veggel, F. C. J. M.; Reinhoudt, D. N. *Phys. Rev. Lett.* **2003**, *89*, 21.
- (24) Oae, S.; Togo, H. *Tetrahedron Lett.* **1982**, *23*, 4701.
- (25) Brust, M.; Walker, M.; Bethell, D.; Schiffrin, D. J.; Whyman, R. *J. Chem. Soc., Chem. Commun.* **1994**, *104*, 801.
- (26) Bystol, A. J.; Campiglia, A. D.; Gillispie, G. D. *Appl. Spectrosc.* **2000**, *54*, 910.
- (27) Bystol, A. J.; Campiglia, A. D.; Gillispie, G. D. *Anal. Chem.* **2001**, *73*, 5762.
- (28) Lakowicz, J. R. *Principles of Fluorescence Spectroscopy*, 2nd ed.; Kluwer Academic: New York, 1999.
- (29) Miller, J. C.; Miller, J. N. *Statistics for Analytical Chemistry*; Wiley: New York, 1984.
- (30) Gersten, J.; Nitzan, A. *J. Chem. Phys.* **1981**, *75*, 1139.
- (31) Gerner, H.; Schulte-Frohlinde, D. *J. Phys. Chem.* **1978**, *82*, 2653.